Quantum Chemical Prediction of Redox Reactivity and Degradation Pathways for Aqueous Phase Contaminants: An Example with HMPA

ARTICLE *in* ENVIRONMENTAL SCIENCE & TECHNOLOGY · AUGUST 2010

Impact Factor: 5.33 · DOI: 10.1021/es1006675 · Source: PubMed

5 AUTHORS, INCLUDING:

Jens Blotevogel
Colorado State University
15 PUBLICATIONS **58** CITATIONS
SEE PROFILE

Thomas Borch
Colorado State University
72 PUBLICATIONS **1,295** CITATIONS
SEE PROFILE

Y. Desyaterik
Colorado State University
33 PUBLICATIONS **525** CITATIONS
SEE PROFILE

Environ. Sci. Technol. **2010,** *44,* 5868–5874

Quantum Chemical Prediction of Redox Reactivity and Degradation Pathways for Aqueous Phase Contaminants: An Example with HMPA

JENS BLOTEVOGEL,[†] THOMAS BORCH,[*,†,‡] YURY DESYATERIK,[§] ARTHUR N. MAYENO,[||] AND TOM C. SALE[⊥]

Departments of Soil and Crop Sciences, Chemistry, Atmospheric Science, Chemical & Biological Engineering, and Civil & Environmental Engineering, Colorado State University, Fort Collins, Colorado 80523

Received March 1, 2010. Revised manuscript received June 11, 2010. Accepted June 23, 2010.

Models used to predict the fate of aqueous phase contaminants are often limited by their inability to address the widely varying redox conditions in natural and engineered systems. Here, we present a novel approach based on quantum chemical calculations that identifies the thermodynamic conditions necessary for redox-promoted degradation and predicts potential degradation pathways. Hexamethylphosphoramide (HMPA), a widely used solvent and potential groundwater contaminant, is used as a test case. Its oxidation is estimated to require at least iron-reducing conditions at low to neutral pH and nitrate-reducing conditions at high pH. Furthermore, the transformation of HMPA by permanganate is predicted to proceed through sequential *N*-demethylation. Experimental validation based on LC/TOF-MS analysis confirms the predicted pathways of HMPA oxidation by permanganate to phosphoramide via the formation of less methylated as well as singly and multiply oxygenated reaction intermediates. Pathways predicted to be thermodynamically or kinetically unfavorable are similarly absent in the experimental studies. Our newly developed methodology will enable scientists and engineers to estimate the favorability of contaminant degradation at a specific field site, suitable approaches to enhance degradation, and the persistence of a contaminant and its reaction intermediates.

Introduction

Due to the vast number of anthropogenic chemicals in the environment and their potential adverse health effects, environmental fate predictions have become an indispensable component of risk assessment today (*1*). Furthermore, theoretical models that predict unknown physicochemical properties or biogeochemical reactivity are used to preassess newly developed compounds in order to identify environmental effects prior to large-scale production and commercialization (*2*). Currently, standard risk assessment strategies most frequently involve predictions based on quantitative structure−activity relationships (QSARs) (*3*). These approaches are attractive since they generate results with minimal computational costs once the relationship and descriptor values have been determined. However, the utility of QSARs is constrained as they rely on experimental databases and are often only valid for narrow ranges of conditions that do not necessarily cover the widely varying redox settings of natural and engineered environments.

Thermodynamic properties ultimately govern the persistence or degradability of a compound in the environment. For many contaminants of concern, however, information on Gibbs free energies of formation or reaction in aqueous phase is unavailable, leading researchers to estimate fundamental thermodynamic properties (*4, 5*) to assess the favorability of transformations or to predict degradation pathways (*6*−*8*). In recent years, increases in computational speed have enabled thermodynamic predictions based on quantum chemical calculations for molecules or systems comprising up to a few hundred atoms (*9*). These approaches allow for accurate investigation of chemicals without any previous knowledge on the substance. Furthermore, quantum chemical models can be used to generate kinetic information, such as activation energies and reaction rates (*10, 11*). This strategy has been widely applied to identify reaction mechanisms and primary degradation pathways when multiple pathways are possible (*12*−*16*).

The fate of a contaminant in groundwater, however, will also depend on the redox conditions in an aquifer (*17, 18*). Consequently, in many in situ remedial approaches, the redox conditions are manipulated by the delivery of strong oxidants or reductants in order to enable or enhance the degradation of redox-sensitive contaminants. For inorganic compounds, readily applicable thermodynamic equilibrium models are already available (ref *19* and references therein). Strategies to assess the redox reactivity of organic contaminants, on the other hand, are very limited. Several quantum chemical methods used for calculation of standard redox potentials have been developed (ref *20* and references therein). One of the most popular approaches is the application of the Born−Haber cycle, in which the free energy of a half reaction is determined from the free energy of reaction in gas phase and solvation free energies of the oxidized and reduced species (*21*). This approach, however, requires the inclusion of at least two explicit hydration shells to yield accurate predictions, which substantially increases the computational cost (*22*). Namazian and co-workers (*23, 24*) calculated standard redox potentials for organic compounds based on the quantum chemically predicted free energy of reaction and a known experimental redox potential for one of the constituent half reactions, thus eliminating the need of explicit solvation by using less costly implicit solvation models. However, no attempts have so far been made to include the influence of pH on redox reactivity in predictive models and use this information to elucidate the conditions necessary for contaminant degradation.

In this article, we present a novel quantum chemical approach to predict the fate of aqueous phase contaminants in natural and engineered environments. The calculations are based on density functional theory (DFT) which allows for a practical balance between accuracy and computational efficiency, compared to the accurate but more expensive

* Corresponding author phone: (970)491-6235; fax: (970)491-0564; e-mail: thomas.borch@colostate.edu. Corresponding author address: Department of Soil and Crop Sciences, 1170 Campus Delivery, Colorado State University, Fort Collins, Colorado 80523-1170.
† Department of Soil and Crop Sciences.
‡ Department of Chemistry.
§ Department of Atmospheric Science.
|| Department of Chemical & Biological Engineering.
⊥ Department of Civil & Environmental Engineering.

10.1021/es1006675

Published on Web 07/07/2010

post-Hartree−Fock ab initio methods (*25*). The specific objectives of this work are to predict chemical reactivity under different redox conditions, potential degradation pathways, and contaminant persistence.

Hexamethylphosphoramide (HMPA), a water-miscible, colorless liquid which is widely used as solvent for polymers and organo-metallic compounds (*26*), is used as a test compound for development and validation of the predictive methodology. HMPA has been detected in groundwater in the U.S. (*27*) and thus represents a contaminant of potential concern. It has been shown to induce nasal tumors in rats and mutagenic effects in fruit flies (*28*). Pentamethylphosphoramide (PMPA), tetramethylphosphoramide (TetMPA), and trimethylphosphoramide (TriMPA) have been detected as metabolites in the same two species (*29*). Terry and Bořkovec investigated the oxidation of HMPA by permanganate and H_2O_2 and identified formylated reaction intermediates in addition to PMPA (*30*). In these studies, the generation of a hydroxymethyl intermediate was suggested but not verified due to the lack of appropriate analytical techniques. No further information about the environmental fate of HMPA has been reported. The consequence of our limited knowledge regarding HMPA, as with innumerable other anthropogenic compounds, is a need to develop advanced tools to assess contaminant fate under natural and engineered conditions.

Computational Details

Quantum chemical calculations were conducted to predict thermodynamic and kinetic parameters for HMPA fate prediction. All calculations were performed using the Gaussian 03 program package without symmetry constraints and with default settings unless otherwise noted. Standard Gibbs free energies of reaction in aqueous phase ($\Delta_r G^0_{(aq)}$) were determined at the restricted B3LYP level of theory with the 6-311++G(d,p) basis set for the elements P, O, N, C, and H as well as the effective core potential (ECP)-type basis set LANL2DZ for Mn. For the $MnO_4^-/HMnO_4^{2-}$ redox couple, one explicit water molecule was found to stabilize the ground state structures and was thus included in the calculations. Inclusion of additional explicit water molecules did not change the free energies of reaction. For the MnO_4^-/MnO_3^- redox couple, explicit solvation had no effect on the free energies of reaction and was thus not considered. The integral equation formalism polarizable continuum model (IEFPCM) was used to account for implicit solvation effects on aqueous species (*31*). Due to the use of UA0 cavity radii, the thermal correction to Gibbs free energy including the zero-point correction from a frequency analysis was added to the total free energy in solution. All aqueous phase free energies were converted to standard state conditions by adding a free-energy change of $RT\ln(24.5) = +7.9$ kJ/mol due to the concentration change from gas to aqueous phase. Free energies of reaction at pH 7 were determined via $\Delta_r G'^0_{(aq)} = \Delta_r G^0_{(aq)} + RT\ln Q$, where Q is the reaction quotient. Potential energy minima were verified by frequency calculations (i.e., no imaginary frequencies). Conformational analyses of the potential energy surfaces were not performed.

Transition state (TS) structures were first optimized at the unrestricted B3LYP level of theory with a 6-31G(d) basis set on C, H, N, and O and a 6-31G(2d) basis set on P and verified by both intrinsic reaction coordinate (IRC) and frequency calculations (i.e., exactly one imaginary frequency). Explicit water molecules were then sequentially added to the TS optimizations until the determined free energies of activation stabilized. Due to the well-documented convergence problems that plague polarizable continuum models (PCM) (*32, 33*) as well as the observation that the effects of *implicit* solvation only negligibly change the molecular properties found in gas phase (*32, 34*), TS optimizations, frequency, and IRC calculations were initially performed without the use of IEFPCM. Only the lowest-energy TS structure for each reaction mechanism including explicit solvation was then optimized at the unrestricted B3LYP level of theory with a 6-31+G(d) basis set on C, H, N, and O and a 6-31+G(2d) basis set on P and verified by both frequency (at 22 °C) and IRC calculations. Subsequently, single point energy calculations on the optimized TS structures were performed at the B3LYP/6-311++G(3df,3pd) level of theory in combination with IEFPCM.

The reaction half-life ($t_{1/2}$) was calculated from the Gibbs free energy of activation in aqueous phase ($\Delta^‡G_{(aq)}$) at 22 °C (same temperature as our experimental system) via transition state theory (*35*)

$$t_{1/2} = \frac{\ln(2)}{k} = \frac{\ln(2)}{\left[\kappa\left(\frac{k_B T}{h}\right)\exp\left(\frac{-\Delta^‡ G_{(aq)}}{RT}\right)\right]}$$

where k is the first-order rate constant, k_B is the Boltzmann constant, T is the temperature in Kelvin, h is Planck's constant, R is the universal gas constant, and κ is the transmission coefficient which accounts for quantum mechanical tunneling effects

$$\kappa = 1 + \frac{1}{24}\left(\frac{1.44\nu_i}{T}\right)^2$$

where ν_i is the magnitude of the imaginary frequency (cm^{-1}) corresponding to the reaction coordinate at the transition state.

Experimental Section

HMPA Oxidation Experiments. Oxidation of HMPA by permanganate was investigated experimentally to test the quantum chemical predictions. In a 1-L Pyrex media glass bottle, an 800 mL solution containing 0.25 mM HMPA (99%, MP Biomedicals) and 6 mM $KMnO_4$ was prepared in 30 mM phosphate buffer at pH 7.0. A parallel control experiment was set up in the absence of $KMnO_4$. The bottles were sealed with PTFE-faced silicone septa and stirred on a magnetic stir plate (240 rpm) at ambient temperature (22 °C). For liquid chromatography - (electrospray ionization) - time-of-flight - mass spectrometry (LC/TOF-MS) analyses (see Analytical Methods below), samples (0.2 mL) were quenched by adding 1.8 mL of 3 mM $Na_2S_2O_3$ and filtered (0.2 μm, nylon). Storage of quenched and filtered samples at ambient temperature over a period of one week revealed that all oxidation reactions were halted. Samples (3 mL) for formaldehyde analysis were quenched with 80 μL of 1 M $Na_2S_2O_3$ and filtered (as above). Formaldehyde was derivatized with 2,4-dinitrophenylhydrazine dissolved in acetonitrile and phosphoric acid at pH 4 and extracted with chloroform. For total nitrogen analyses, 10-mL samples were quenched with 300 μL of 1 M $Na_2S_2O_3$ and filtered (as above). For carbinolamides ($HOCH_2NRP$), a rapid (nonoxidative) decomposition was observed after quenching. Thus, due to the high sampling frequency, the oxidation experiments were performed one at a time to allow for immediate analyses. This experiment was conducted three times, verifying the reproducibility of the observations made. The analytical results will be presented in another paper.

HMPA Hydrolysis Experiments. To investigate the reactivity of HMPA in the absence of a strong oxidant, phosphate buffered (30 mM; pH 7.0) DI water (800 mL) in 1-L Pyrex media glass bottles sealed with a PTFE-faced silicone septum were prepared in triplicate and autoclaved. HMPA was then injected to yield a final concentration of 0.25 mM. The reaction bottles were stored in the dark without agitation at ambient temperature (22 °C). 150-μL samples

were diluted 1:10 with DI water and analyzed monthly by LC/TOF-MS.

Analytical Methods. HMPA and its phosphoramide-containing transformation products were analyzed with an Agilent 1100 Series liquid chromatograph equipped with a 150 mm ×2.1 mm XTerra phenyl column, 3.5 μm particle size (Waters) in combination with an Agilent G3250AA MSD TOF system (LC/MS-TOF). The injection volume was 10 μL, and the flow rate was 0.5 mL/min. During the first three hours of the HMPA oxidation experiment (i.e., while HMPA was detectable) and for the HMPA hydrolysis experiment, separation was carried out isocratically with 0.01% formic acid in water/acetonitrile (98:2). For the samples obtained three hours after initiation of the HMPA oxidation experiment, chromatographic separation was carried out isocratically with 0.01% formic acid in water. The capillary and fragmentation voltages were 2.8 kV and 140 V, respectively. The mass analyzer was calibrated from m/z 90 to 600 in positive ionization mode. For the detection of carboxylic acids, samples were analyzed in negative ionization mode, using the same parameters, except for capillary voltage (2.0 kV). Besides HMPA, reference standards were only available for PMPA, TetMPA, and TriMPA (all custom synthesized and generously provided by DuPont, 97% purity). The limits of detection (LOD) were 0.039 μM, 0.070 μM, 0.17 μM, and 0.18 μM, respectively.

Oxidation−reduction potential (ORP) and pH were measured with a UP-25 pH/mV/Ion Meter (Denver Instruments). Total nitrogen was quantified with a TNM-1 Total Nitrogen Measuring Unit connected to a TOC-V CSH Total Organic Carbon Analyzer (both Shimadzu). Formaldehyde analyses were carried out on a 5890 Series II gas chromatograph (Hewlett-Packard) equipped with a flame ionization detector, using a method modified from Dalene et al. (*36*). The LOD for formaldehyde was 0.27 μM.

Results

Prediction of Contaminant Reactivity Under Different Redox Conditions. To identify the thermodynamic conditions favoring HMPA oxidation, stability lines were determined, based on quantum chemically calculated free energies of reaction, and superimposed onto stability (Pourbaix) diagrams (Figure 1). Initial oxidation of HMPA can occur at the methyl substituent, to give hydroxymethyl-pentamethylphosphoramide (HM-PMPA, compound 4 in Figure 2), and at the nitrogen atom, to form HMPA *N*-oxide (compound 2 in Figure 2), as previously described (*29*). Since Gibbs free energies for oxidation or reduction half reactions cannot be calculated directly due to the presence of protons and free electrons in the formal half reaction equations, the free energy of reaction for HMPA oxidation by hydrogen peroxide was calculated first

$$\text{HMPA} + \text{H}_2\text{O}_2 = \text{HM-PMPA} + \text{H}_2\text{O} \quad \Delta_r G^0_{(aq)} = -268 \text{ kJ/mol}$$

$$\text{HMPA} + \text{H}_2\text{O}_2 = \text{HMPA } N\text{-oxide} + \text{H}_2\text{O} \quad \Delta_r G^0_{(aq)} = -31 \text{ kJ/mol}$$

The known half reaction for H_2O_2 reduction (*37*)

$$\text{H}_2\text{O}_2 + 2\text{H}^+ + 2\text{e}^- = 2\text{H}_2\text{O} \quad \Delta_r G^0_{(aq)} = -342 \text{ kJ/mol}$$

was then subtracted, yielding the HMPA oxidation half reactions and, consequently, the stability lines for the respective HMPA redox couples (for details, see the Supporting Information)

$$\text{HM-PMPA} + 2\text{H}^+ + 2\text{e}^- = \text{HMPA} + \text{H}_2\text{O} \quad p\varepsilon = 6.5 - \text{pH}$$

$$\text{HMPA } N\text{-oxide} + 2\text{H}^+ + 2\text{e}^- = \text{HMPA} + \text{H}_2\text{O} \quad p\varepsilon = 27.3 - \text{pH}$$

These equations describe the gray-white boundaries in Figure 1 that separate favorable and unfavorable conditions for HMPA oxidation.

The stability diagrams reveal that HMPA oxidation to HM-PMPA (Figure 1a) is favorable in the presence of strong oxidants typically used for in situ groundwater remediation. The process is also favorable under naturally occurring aerobic and nitrate-reducing conditions. Under iron-reducing conditions, oxidation to HM-PMPA is favorable only at neutral and lower pH values, depending on the total Fe and carbonate concentrations (here: 10^{-5} M and 10^{-3} M, respectively). Under sulfate-reducing and methanogenic conditions, this reaction is thermodynamically unfavorable. For the oxidation to HMPA *N*-oxide (Figure 1b), only very strong oxidants, such as H_2O_2 and ozone, may lead to transformation.

Prediction of Potential Contaminant Degradation Pathways. Based on the results of the stability diagrams, the common remediation agent permanganate (MnO_4^-) was chosen as the model oxidant with which to further investigate potential HMPA degradation pathways and products. A hypothetical degradation pathway was created based on expert knowledge (Figure 2), and the thermodynamic favorability of possible oxidation reactions as well as redox-independent decomposition and hydrolysis reactions was calculated, as described in the Computational Details section. The determined aqueous free energies of reaction at neutral pH predict that HMPA can be oxidized at the methyl substituent to form HM-PMPA via hydride abstraction by MnO_4^-, in accordance with the reported mechanism of alkyl substituent oxidation by permanganate (*38*), where the

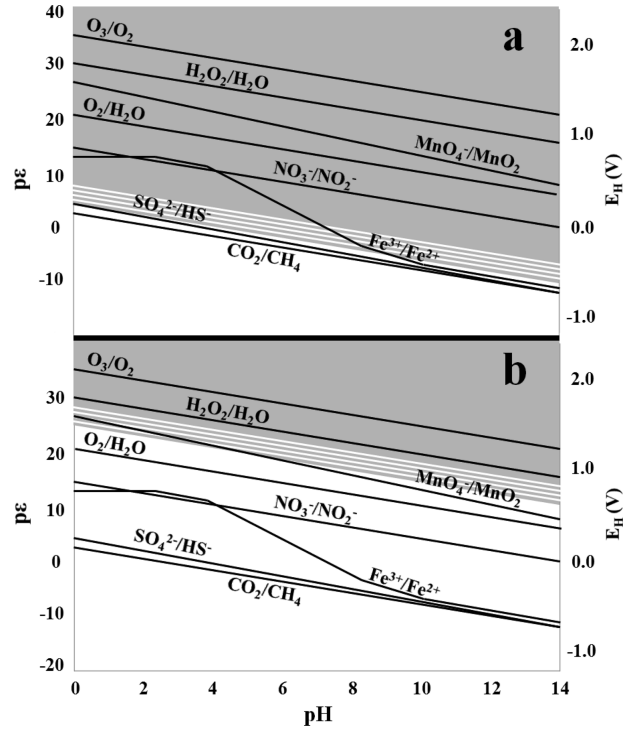

FIGURE 1. (a) Stability diagram for the HMPA/hydroxymethyl-PMPA redox couple. (b) Stability diagram for the HMPA/HMPA *N*-oxide redox couple. HMPA oxidation is unfavorable under conditions represented by white fields and favorable under conditions represented by gray fields. The gray-white hatched areas separating the stability fields reflect uncertainty associated with the estimated error range of the prediction (±0.1 V). All stability lines were adapted from ref *37* and represent standard conditions except [Fe] = 10^{-5} M and $[C]_{inorg}$ = 10^{-3} M for the iron redox couple.

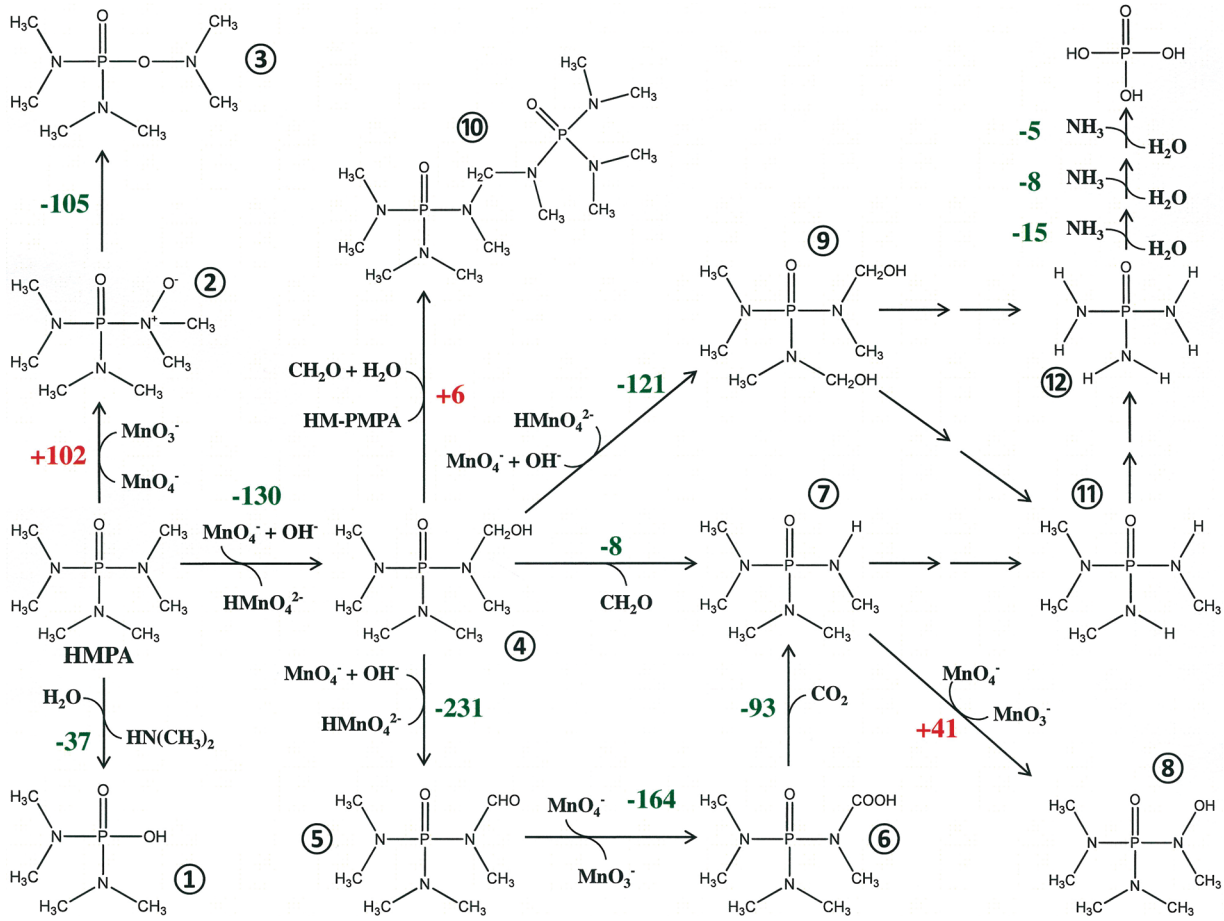

FIGURE 2. Potential degradation pathway for HMPA in permanganate-containing solution showing the predicted aqueous free energies of reaction (kJ/mol) at pH 7. Free energies are marked (−) green for favorable and (+) red for unfavorable transformations.

oxygen in the hydroxymethyl substituent stems from the solvent water. Furthermore, the calculations indicate that hydrolysis of HMPA to tetramethylphosphoric diamide (compound 1 in Figure 2) and dimethylamine is thermodynamically favorable, whereas oxidation at the nitrogen atom to form HMPA *N*-oxide is unfavorable, in agreement with the predicted stability diagram (Figure 1b).

For the transformation of HM-PMPA, three reactions were calculated to be favorable, as indicated by negative free energies of reaction: oxidation to dihydroxymethyl-TetMPA (compound 9 in Figure 2), oxidation to formyl-PMPA (compound 5 in Figure 2) via hydride abstraction from the deprotonated alkoxide (*39*), and decomposition to formaldehyde and PMPA (compound 7 in Figure 2). However, the combination of two HM-PMPA molecules to form the condensation product *N,N‴*-methylenebis[pentamethylphosphoramide] (compound 10 in Figure 2), formaldehyde, and water, as previously observed during distillation of HM-PMPA (*40*), was calculated to be unfavorable under standard conditions in water at neutral pH.

For formyl-PMPA, oxidation to carboxyl-PMPA (compound 6 in Figure 2) with subsequent decarboxylation to PMPA was calculated to be favorable. The oxidation mechanism for the formyl substituent leading to the formation of a carboxylic acid was assumed to proceed via oxygen transfer from MnO_4^- to yield MnO_3^- as previously shown for the oxidation of various aldehydes using ^{18}O-labeled permanganate (*41, 42*). Oxidation of formyl-PMPA to formyl-hydroxymethyl-TetMPA was also calculated to be exergonic ($\Delta_r G^0_{(aq)} = -130$ kJ/mol; not shown in Figure 2 for simplicity).

Oxidation at the demethylated nitrogen atom is unfavorable for PMPA; rather, PMPA is oxidized to hydroxymethyl-TetMPA ($\Delta_r G^0_{(aq)} = -128$ kJ/mol; not shown in Figure 2), analogous to HMPA oxidation by permanganate.

Thus, the overall transformation of HMPA in permanganate-containing solution is predicted to proceed through oxidative *N*-demethylation via the formation of less methylated intermediates, such as PMPA, TetMPA (compound 11 in Figure 2), TriMPA, and so forth, as well as singly-, doubly-, and possibly more highly oxygenated phosphoramide-based compounds to eventually yield phosphoramide (compound 12 in Figure 2). Subsequently, phosphoramide may hydrolyze through three sequential deamination steps, leading to the formation of *o*-phosphate and ammonia. Phosphoramide hydrolysis has been reported to occur under all pH conditions (*43*).

Experimental Validation. Qualitative LC/MS-TOF analysis of samples from the HMPA oxidation experiment confirmed the predictions made based on the free energy calculations. None of the thermodynamically unfavorable transformation products were detected. Aside from the nonoxygenated intermediates such as PMPA, TetMPA, and TriMPA, a variety of oxygenated compounds were observed (Table 1). These included mono-, di-, and tri- hydroxymethyl and/or formyl-PMPA, TetMPA and TriMPA as well as minor amounts of carboxyl-PMPA over the course of 46 h. The chromatographic peak areas revealed that none of these intermediates were accumulating. Analysis for phosphoramide, at day 14 post-reaction start, revealed its presence (data not shown).

Quantitative analysis of HMPA, PMPA, TetMPA, and TriMPA, the four compounds where references were available, demonstrated that HMPA is rapidly oxidized by permanganate, becoming undetectable after 3 h of reaction. The

TABLE 1. LC/MS-TOF Data for HMPA and Its Major Transformation Products Detected during the 46-h Permanganate Oxidation Experiment

compound (number in Figure *2*)	retention time (min)	base peak	base peak formula	observed *m/z*	theoretical *m/z*	error (ppm)
			ESI Positive			
HMPA	11.3[a]	$[M+H]^+$	$C_6H_{19}N_3OP^+$	180.1294	180.1267	15.0
formyl-PMPA (*5*)	4.1[a]; 10.1[b]	$[M+H]^+$	$C_6H_{17}N_3O_2P^+$	194.1082	194.1060	11.3
HM-PMPA (*4*)	3.9[a]; 9.1[b]	$[M+H]^+$-H_2O	$C_6H_{17}N_3OP^+$	178.1131	178.1111	11.2
PMPA (*7*)	3.3[a]; 7.0[b]	$[M+H]^+$	$C_5H_{17}N_3OP^+$	166.1131	166.1111	12.0
diformyl-TetMPA	2.3[a]; 3.6[b]	$[M+H]^+$	$C_6H_{15}N_3O_3P^+$	208.0849	208.0852	–1.4
formyl-HM-TetMPA	2.0[a]; 3.3[b]	$[M+H]^+$-H_2O	$C_6H_{15}N_3O_2P^+$	192.0902	192.0903	–0.5
formyl-TetMPA	3.1[b]	$[M+H]^+$	$C_5H_{15}N_3O_2P^+$	180.0909	180.0903	3.3
diHM-TetMPA (*9*)	1.9[a]; 2.9[b]	$[M+H]^+$-H_2O	$C_6H_{17}N_3O_2P^+$	194.1086	194.1060	13.4
HM-TetMPA	2.6[b]	$[M+H]^+$-H_2O	$C_5H_{15}N_3OP^+$	164.0980	164.0954	15.8
TetMPA (*11*)	1.7[a]; 2.4[b]	$[M+H]^+$	$C_4H_{15}N_3OP^+$	152.0974	152.0954	13.1
formyl-diHM-TriMPA	1.5[b]	$[M+H]^+$-H_2O	$C_6H_{15}N_3O_3P^+$	208.0854	208.0852	1.0
formyl-HM-TriMPA	1.5[b]	$[M+H]^+$-H_2O	$C_5H_{13}N_3O_2P^+$	178.0750	178.0746	2.2
formyl-TriMPA	1.4[b]	$[M+H]^+$	$C_4H_{13}N_3O_2P^+$	166.0759	166.0746	7.8
TriMPA	1.3[b]	$[M+H]^+$	$C_3H_{13}N_3OP^+$	138.0794	138.0797	–2.2
			ESI Negative			
carboxyl-PMPA (*6*)	4.1[a]	$[M-H]^-$-CO_2	$C_5H_{15}N_3OP^-$	164.0911	164.0954	–26.2

[a] Mobile phase 0.01% HCOOH in water/ACN (98:2). [b] Mobile phase 0.01% HCOOH in water.

nonoxygenated intermediates PMPA, TetMPA, and TriMPA were all detected, however, at molar concentrations less than 3% of the initial 0.25 mM HMPA concentration at all time points sampled. Thus, compounds oxygenated at one or more methyl substituents comprised the majority of the oxidation products during the initial 46 h of HMPA degradation. Analysis of total nitrogen in the aqueous phase revealed that volatilization and sorption were negligible. Both the pH (7.0) and the ORP (0.63 V) remained constant throughout the experiment (data not shown).

Formaldehyde was also detected (at concentrations below 10 μM), indicating that the decomposition of hydroxymethyl-containing intermediates (Figure 2) was indeed occurring.

In the control experiments without permanganate, HMPA concentrations remained constant, and neither phosphoramide-containing reaction intermediates nor formaldehyde were detected. This stability was further confirmed by the HMPA hydrolysis experiments, where no transformation was observed over the course of six months (see the Experimental Section).

Prediction of Contaminant Persistence. To predict the persistence of HMPA in the absence of a strong oxidant, the rate of HMPA hydrolysis was estimated by computationally determining transition states and identifying the lowest energy TS, which likely corresponds to the kinetically most favorable pathway. Four potential mechanisms were considered, each of which had previously been proposed for hydrolysis of tetracoordinate phosphorus compounds: a stepwise dissociative mechanism (elimination-addition) with a tricoordinate intermediate, a stepwise associative mechanism (addition−elimination) with a pentacoordinate intermediate, and concerted backside and frontside mechanisms with a single pentacoordinate transition state (*44, 45*). At pH 7, the transition state with the lowest energy corresponded to the acid-catalyzed concerted backside nucleophilic attack at phosphorus ($S_N2@P$) mechanism, in agreement with previous experimental findings for phosphorus amides (*43, 45*). A minimum of five explicit water molecules was required in the transition state optimizations before the activation energies stabilized. Based on the calculated free energy of activation of 97 kJ/mol at 22 °C under standard conditions (i.e., pH 0), a half-life of 12,300 years for HMPA hydrolysis at neutral pH is predicted.

Discussion

The redox conditions of an aquifer play a crucial role in the environmental fate of contaminants as the thermodynamic driving force behind their transformation into harmful or innocuous products (*17*). Thus, the prediction of redox reactivity is extremely valuable. For standard conditions, redox potentials have previously been predicted to within 0.3 V using quantum chemical methods (*20, 22, 23*). Here, we describe a quantum chemical approach to estimate the pH-dependence of redox reactivity (Figure 1), based on calculations for the respective contaminant and known half reactions for electron acceptors and donors typically occurring in aqueous environments. This approach circumvents the consideration of explicit solvation effects, allowing for substantially faster computations compared to other approaches (see the Introduction) (*20, 22*). The accuracy of the calculated B3LYP reaction energies is estimated to be within 10−20 kJ/mol (*46*), corresponding to a redox potential of approximately 0.05−0.1 V for a half-reaction involving two electrons. Each stability line is only valid for the respective redox couple and is independent of the reaction mechanism. To determine the $p\varepsilon$/pH conditions necessary for complete mineralization, one diagram for every redox couple within the degradation pathway, or at least for the redox reaction with the highest free energy, must be generated. In the case of HMPA, this is the initial oxidation of the methyl substituent, as the oxidation reactions of the alcoholic and aldehydic substituents have lower free energies of reaction and thus may proceed at lower redox potentials. Moreover, the diagrams in Figure 1 were calculated for standard conditions (i.e., 1 M concentrations for all species at 25 °C), which are not representative of typical conditions in aqueous environments. However, the true concentrations of both contaminants and electron acceptors or donors at a particular field site can be taken into account by simply adding the well-known term $RT \ln Q$ to the standard free energies. A specific temperature can also easily be incorporated in the quantum chemical calculations. This is important for the assessment of redox reactivity, especially when two stability lines are closely spaced.

The prediction of potential degradation pathways initially requires expert knowledge. All possible transformations must be identified so that favorable reaction products are not overlooked. Subsequently, the calculation of aqueous free

energies of reaction at, for example, groundwater-typical pH values, can be used to exclude thermodynamically unfavorable reactions, such as HMPA oxidation at the nitrogen atom by permanganate. Again, care must be taken since standard conditions do not accurately characterize contaminated field sites, where the parent compound is initially the predominant species. For reactions with slightly positive free energies, the concentrations of all species participating in the reaction need to be considered via addition of *RT ln Q*. For instance, the formation of *N,N‴*-methylenebis[pentamethylphosphoramide] from HM-PMPA ($\Delta_r G'^0_{(aq)} = +6$ kJ/mol) can become favorable when HM-PMPA is present in excess. In addition, the estimated error of 10−20 kJ/mol for the B3LYP reaction energies prevents reliable exclusion of this reaction. In this specific case, however, the condensation product *N,N‴*-methylenebis[pentamethylphosphoramide] was not detected in our system, as expected, due to the different experimental conditions (*40*).

The predictions of both redox reactivity (Figure 1) and potential degradation pathways (Figure 2) are based solely on thermodynamic calculations. Kinetic constraints, however, are not considered; therefore, reactions calculated to be thermodynamically favorable may still not proceed on a practical time scale due to high activation barriers. For example, although hydrolysis of HMPA is thermodynamically favorable ($\Delta_r G'^0_{(aq)} = -37$ kJ/mol), the calculated half-life of 12,300 years indicates persistence in water at neutral pH in the absence of a suitable oxidant. Acidic or basic conditions, however, would alter the degradation kinetics.

It has to be noted that activation barriers calculated via the popular B3LYP functional are typically underestimated (*47*). Other DFT methods, such as MPWB1K (*47*) or BB1K (*48*), may yield more accurate predictions for thermochemical kinetics. A potential underestimation of activation barriers corresponds to an underestimation of reaction half-lives and would thus imply that a contaminant is even more persistent than predicted.

When calculating free energies of activation in aqueous phase, consideration of all possible reaction mechanisms (or, alternatively, thorough scans of the potential energy surface) as well as inclusion of explicit water molecules are of paramount importance. If the lowest-energy transition state is not correctly identified, reaction half-lives will be overestimated. Unlike activation energies, free energies of reaction can be accurately computed using less costly implicit solvation models (*33*). These account for long-range bulk solvent−solute interactions such as electrostatic effects but not for short-range effects such as hydrogen bonding (*31, 32, 49*), which may be important in TS calculations.

Implications for the Environmental Fate of HMPA. The degradation of HMPA requires the presence of suitable oxidants, as hydrolysis is hindered by a high activation barrier at neutral pH. HMPA is rapidly oxidized to phosphoramide by the common remediation agent permanganate via sequential *N*-demethylation. Subsequently, phosphoramide hydrolyzes to ammonia and *o*-phosphate (*43*). Using LC/MS-TOF, we have demonstrated for the first time that HMPA oxidation by permanganate does proceed through the formation of hydroxymethylated compounds. Furthermore, a carboxylated intermediate was detected, which had not been observed previously by Terry and Bořkovec (*30*). The application of stronger oxidants such as ozone may, however, favor a different degradation pathway, such as oxidation at the nitrogen atom, producing HMPA *N*-oxide and its rearrangement product ((bis(dimethylamino)phosphinyl)oxy-)dimethylamine (compound 3 in Figure 2) (*50*). In conclusion, based on our quantum chemical predictions, HMPA-contaminated water can be successfully remediated through the application of permanganate without accumulation of persistent reaction intermediates.

Implications for Contaminant Fate Prediction. The quantum chemical methodology we have presented here can be used by scientists and engineers to predict the fate of both organic and inorganic contaminants as a function of redox potential and pH in aqueous phases such as groundwater. This novel method overcomes many limitations of standard QSAR approaches. The quantum chemical determination of stability lines can serve as a powerful screening tool to assess whether the natural conditions at a specific field site favor contaminant transformation. This determination can also identify the type of redox-active remediation agents that can be used to enhance or enable degradation. The calculation of aqueous free energies of reaction allows for the identification of potential degradation products and the exclusion of unfavorable transformation pathways. Finally, kinetics and therefore the persistence of a contaminant and its degradation products can also be estimated, along with primary degradation pathways, based on calculated activation energies. The prediction of primary degradation pathways is part of our ongoing studies.

Acknowledgments

This paper is dedicated to the memory of David M. Gilbert. Primary funding for this work was provided by E.I. du Pont de Nemours and Company. Complementary support was provided by the University Consortium for Field-Focused Groundwater Contamination Research, a National Science Foundation (NSF) CAREER Award (EAR 0847683) to T. B., and NCSA through TeraGrid resources. We thank Don Dick and Richard Casey for their invaluable help on this project.

Supporting Information Available

Calculation of stability lines. This material is available free of charge via the Internet at http://pubs.acs.org.

Literature Cited

(1) Cronin, M. T. D.; Walker, J. D.; Jaworska, J. S.; Comber, M. H. I.; Watts, C. D.; Worth, A. P. Use of QSARs in international decision-making frameworks to predict ecologic effects and environmental fate of chemical substances. *Environ. Health Perspect.* **2003**, *111*, 1376–1390.

(2) Bennett, E. R.; Clausen, J.; Linkov, E.; Linkov, I. Predicting physical properties of emerging compounds with limited physical and chemical data: QSAR model uncertainty and applicability to military munitions. *Chemosphere* **2009**, *77*, 1412–1418.

(3) Boethling, R. S.; Mackay, D. *Handbook of Property Estimation Methods for Chemicals: Environmental and Health Sciences*; CRC Press: Boca Raton, 2000.

(4) Dolfing, J.; Harrison, B. K. Gibbs free-energy of formation of halogenated aromatic-compounds and their potential role as electron-acceptors in anaerobic environments. *Environ. Sci. Technol.* **1992**, *26*, 2213–2218.

(5) Holmes, D. A.; Harrison, B. K.; Dolfing, J. Estimation of Gibbs free-energies of formation for polychlorinated-biphenyls. *Environ. Sci. Technol.* **1993**, *27*, 725–731.

(6) Beurskens, J. E. M.; Dekker, C. G. C.; Vandenheuvel, H.; Swart, M.; Dewolf, J. Dechlorination of chlorinated benzenes by an anaerobic microbial consortium that selectively mediates the thermodynamic most favorable reactions. *Environ. Sci. Technol.* **1994**, *28*, 701–706.

(7) Huang, C. L.; Harrison, B. K.; Madura, J.; Dolfing, J. Gibbs free energies of formation of PCDDs: Evaluation of estimation methods and application for predicting dehalogenation pathways. *Environ. Toxicol. Chem.* **1996**, *15*, 824–836.

(8) Woods, S. L.; Trobaugh, D. J.; Carter, K. J. Polychlorinated biphenyl reductive dechlorination by vitamin B-12s: Thermodynamics and regiospecificity. *Environ. Sci. Technol.* **1999**, *33*, 857–863.

(9) Siegbahn, P. E. M. The performance of hybrid DFT for mechanisms involving transition metal complexes in enzymes. *J. Biol. Inorg. Chem.* **2006**, *11*, 695–701.

(10) Lei, W. F.; Zhang, R. Y.; McGivern, W. S.; Derecskei-Kovacs, A.; North, S. W. Theoretical study of OH-O_2-isoprene peroxy radicals. *J. Phys. Chem. A* **2001**, *105*, 471–477.

(11) Zhang, Q. Z.; Li, S. Q.; Qu, X. H.; Shi, X. Y.; Wang, W. X. A quantum mechanical study on the formation of PCDD/Fs from 2-chlorophenol as precursor. *Environ. Sci. Technol.* **2008**, *42*, 7301–7308.
(12) Fueno, H.; Tanaka, K.; Sugawa, S. Theoretical study of the dechlorination reaction pathways of octachlorodibenzo-p-dioxin. *Chemosphere* **2002**, *48*, 771–778.
(13) Kılıç, M.; Koçtürk, G.; San, N.; Çınar, Z. A model for prediction of product distributions for the reactions of phenol derivatives with hydroxyl radicals. *Chemosphere* **2007**, *69*, 1396–1408.
(14) Nonnenberg, C.; van der Donk, W. A.; Zipse, H. Reductive dechlorination of trichloroethylene: A computational study. *J. Phys. Chem. A* **2002**, *106*, 8708–8715.
(15) Özen, A. S.; Aviyente, V.; Klein, R. A. Modeling the oxidative degradation of azo dyes: A density functional theory study. *J. Phys. Chem. A* **2003**, *107*, 4898–4907.
(16) Zhang, Q. Z.; Qu, X. H.; Wang, W. X. Mechanism of OH-initiated atmospheric photooxidation of dichlorvos: A quantum mechanical study. *Environ. Sci. Technol.* **2007**, *41*, 6109–6116.
(17) Borch, T.; Kretzschmar, R.; Kappler, A.; Cappellen, P. V.; Ginder-Vogel, M.; Voegelin, A.; Campbell, K. Biogeochemical redox processes and their impact on contaminant dynamics. *Environ. Sci. Technol.* **2010**, *44*, 15–23.
(18) Christensen, T. H.; Bjerg, P. L.; Banwart, S. A.; Jakobsen, R.; Heron, G.; Albrechtsen, H. J. Characterization of redox conditions in groundwater contaminant plumes. *J. Contam. Hydrol.* **2000**, *45*, 165–241.
(19) Meeussen, J. C. L. ORCHESTRA: An object-oriented framework for implementing chemical equilibrium models. *Environ. Sci. Technol.* **2003**, *37*, 1175–1182.
(20) Roy, L. E.; Jakubikova, E.; Guthrie, M. G.; Batista, E. R. Calculation of one-electron redox potentials revisited. Is it possible to calculate accurate potentials with density functional methods. *J. Phys. Chem. A* **2009**, *113*, 6745–6750.
(21) Li, J.; Fisher, C. L.; Chen, J. L.; Bashford, D.; Noodleman, L. Calculation of redox potentials and pK_a values of hydrated transition metal cations by a combined density functional and continuum dielectric theory. *Inorg. Chem.* **1996**, *35*, 4694–4702.
(22) Uudsemaa, M.; Tamm, T. Density-functional theory calculations of aqueous redox potentials of fourth-period transition metals. *J. Phys. Chem. A* **2003**, *107*, 9997–10003.
(23) Namazian, M.; Almodarresieh, H. A.; Noorbala, M. R.; Zare, H. R. DFT calculation of electrode potentials for substituted quinones in aqueous solution. *Chem. Phys. Lett.* **2004**, *396*, 424–428.
(24) Namazian, M.; Norouzi, P.; Ranjbar, R. Prediction of electrode potentials of some quinone derivatives in acetonitrile. *J. Mol. Struct. THEOCHEM* **2003**, *625*, 235–241.
(25) Ess, D. H.; Houk, K. N. Activation energies of pericyclic reactions: Performance of DFT, MP2, and CBS-QB3 methods for the prediction of activation barriers and reaction energetics of 1,3-dipolar cycloadditions, and revised activation enthalpies for a standard set of hydrocarbon pericyclic reactions. *J. Phys. Chem. A* **2005**, *109*, 9542–9553.
(26) Lloyd, J. W. Hexamethylphosphoric triamide (HMPA). *Am. Ind. Hyg. Assoc. J.* **1975**, *36*, 917–919.
(27) Campos, D. Field demonstration of UV/H_2O_2 on the treatment of groundwater contaminated with HMPA. In *Chemical Oxidation: Technologies for the Nineties*; Eckenfelder, W. W., Bowers, A. R., Roth, J. A., Eds.; Technomic Publishing Company: Lancaster, 1997; Vol. 6, pp 19−26.
(28) Zijlstra, J. A.; Brussee, J.; Vandergen, A.; Vogel, E. W. Importance of multiple hydroxylated metabolites in hexamethylphosphoramide (HMPA)-mediated mutagenesis in *Drosophila melanogaster*. *Mutat. Res.* **1989**, *212*, 193–211.
(29) Jones, A. R.; Jackson, H. Metabolism of hexamethylphosphoramide and related compounds. *Biochem. Pharmacol.* **1968**, *17*, 2247–2252.
(30) Terry, P. H.; Borkovec, A. B. Insect chemosterilants. 4. Oxidation of hexamethylphosphoric triamide and synthesis of N-formylphosphoramides. *J. Med. Chem.* **1968**, *11*, 958–961.
(31) Cances, E.; Mennucci, B.; Tomasi, J. A new integral equation formalism for the polarizable continuum model: Theoretical background and applications to isotropic and anisotropic dielectrics. *J. Chem. Phys.* **1997**, *107*, 3032–3041.
(32) Barone, V.; Cossi, M.; Tomasi, J. A new definition of cavities for the computation of solvation free energies by the polarizable continuum model. *J. Chem. Phys.* **1997**, *107*, 3210–3221.
(33) Stare, J.; Henson, N. J.; Eckert, J. Mechanistic aspects of propene epoxidation by hydrogen peroxide. Catalytic role of water molecules, external electric field, and zeolite framework of TS-1. *J. Chem. Inf. Model.* **2009**, *49*, 833–846.
(34) Nguyen, M. T.; Raspoet, G. The hydration mechanism of ketone: 15 years later. *Can. J. Chem.* **1999**, *77*, 817–829.
(35) Raman, S.; Ashcraft, R. W.; Vial, M.; Klasky, M. L. Oxidation of hydroxylamine by nitrous and nitric acids. Model development from first principle SCRF calculations. *J. Phys. Chem. A* **2005**, *109*, 8526–8536.
(36) Dalene, M.; Persson, P.; Skarping, G. Determination of formaldehyde in air by chemisorption on glass filters impregnated with 2,4-dinitrophenylhydrazine using gas-chromatography with thermionic specific detection. *J. Chromatogr.* **1992**, *626*, 284–288.
(37) Stumm, W.; Morgan, J. J. *Aquatic Chemistry: Chemical Equilibria and Rates in Natural Waters*, 2nd, ed.; John Wiley & Sons: New York, 1996.
(38) Gardner, K. A.; Mayer, J. M. Understanding C-H bond oxidations - H• and H^- transfer in the oxidation of toluene by permanganate. *Science* **1995**, *269*, 1849–1851.
(39) Fatiadi, A. J. The classical permanganate ion - Still a novel oxidant in organic chemistry. *Synthesis-Stuttgart* **1987**, 85–127.
(40) Terry, P. H.; Borkovec, A. B. Insect chemosterilants. 9. N-(hydroxymethyl)-N, N′, N′, N″, N″-pentamethylphosphoric triamide. *J. Med. Chem.* **1970**, *13*, 782–783.
(41) Jaky, M.; Szammer, J. Oxidation of aldehydes with permanganate in acidic and alkaline media. *J. Phys. Org. Chem.* **1997**, *10*, 420–426.
(42) Wiberg, K. B.; Stewart, R. The mechanisms of permanganate oxidation. 1. The oxidation of some aromatic aldehydes. *J. Am. Chem. Soc.* **1955**, *77*, 1786–1795.
(43) Richter, S.; Töpelmann, W.; Lehmann, H.-A. Hydrolysis of phosphoric acid amides. *Z. Anorg. Allg. Chem.* **1976**, *424*, 133–143.
(44) van Bochove, M. A.; Swart, M.; Bickelhaupt, F. M. Nucleophilic substitution at phosphorus centers (S_N2@P). *ChemPhysChem* **2007**, *8*, 2452–2463.
(45) Rahil, J.; Haake, P. Reactivity and mechanism of hydrolysis of phosphonamides. *J. Am. Chem. Soc.* **1981**, *103*, 1723–1734.
(46) Noodleman, L.; Lovell, T.; Han, W. G.; Li, J.; Himo, F. Quantum chemical studies of intermediates and reaction pathways in selected enzymes and catalytic synthetic systems. *Chem. Rev.* **2004**, *104*, 459–508.
(47) Zhao, Y.; Truhlar, D. G. Hybrid meta density functional theory methods for thermochemistry, thermochemical kinetics, and noncovalent interactions: The MPW1B95 and MPWB1K models and comparative assessments for hydrogen bonding and van der Waals interactions. *J. Phys. Chem. A* **2004**, *108*, 6908–6918.
(48) Zhao, Y.; Lynch, B. J.; Truhlar, D. G. Development and assessment of a new hybrid density functional model for thermochemical kinetics. *J. Phys. Chem. A* **2004**, *108*, 2715–2719.
(49) Tomasi, J.; Mennucci, B.; Cammi, R. Quantum mechanical continuum solvation models. *Chem. Rev.* **2005**, *105*, 2999–3093.
(50) Holden, I.; Segall, Y.; Kimmel, E. C.; Casida, J. E. Peracid-mediated *N*-oxidation and rearrangement of dimethylphosphoramides - Plausible model for oxidative bioactivation of the carcinogen hexamethylphosphoramide (HMPA). *Tetrahedron Lett.* **1982**, *23*, 5107–5110.

ES1006675